Investigating the Applicability of a Global Average Calibration Line for Ambient Size-Resolved Cloud Condensation Nuclei (CCN) Measurements: A Technical Note

RIZANA SALIM,[a,b] AISHWARYA SINGH,[a,b] SWETHA S,[c] KAVYASHREE N. KALKURA,[a,b] AMAR KRISHNA GOPINATH,[b,d] SUBHA S. RAJ,[a,b] RAMESHCHAND K. A.,[e] R. RAVI KRISHNA,[b,d] AND SACHIN S. GUNTHE[a,b]

[a] *Department of Civil Engineering, Environmental Engineering Division, Indian Institute of Technology Madras, Chennai, India*
[b] *Laboratory for Atmospheric and Climate Sciences, Indian Institute of Technology Madras, Chennai, India*
[c] *CSIR Fourth Paradigm Institute, Bengaluru, India*
[d] *Department of Chemical Engineering, Indian Institute of Technology Madras, Chennai, India*
[e] *Department of Mechanical Engineering, College of Engineering, Munnar, India*

(Manuscript received 27 July 2022, in final form 9 February 2023, accepted 5 April 2023)

ABSTRACT: Aerosol–cloud–precipitation interaction represents the largest uncertainty in climate change's current and future understanding. Therefore, aerosol properties affecting the cloud and precipitation formation and their accurate estimation is a first step in developing improved parameterizations for the prognostic climate models. Over the last couple of decades, a commercially available Cloud Condensation Nuclei Counter (CCNC) has been deployed in the field and laboratory for characterizing CCN properties of ambient or atmospherically relevant laboratory-generated aerosols. However, most of the CCN measurements performed in the field are often compounded with the erroneous estimation of CCN concentration and other parameters due to a lack of robust and accurate CCNC calibration. CCNC is not a plug-and-play instrument and requires prudent calibration and operation, to avoid erroneous data and added parameterization uncertainties. In this work, we propose and demonstrate the usability of a global calibration equation derived from CCNC calibration experiments from 8 contrasting global environments. Significant correlation was observed between the global calibration and each of the 16 individual experiments. A significant improvement in the correlation was observed when the calibration experiments were separated for high-altitude measurements. Using these equations, we further derived the effective hygroscopicity parameter and found lower relative uncertainty in the hygroscopicity parameter at higher effective supersaturation. Our results signify that altitude-based pressure change could be of importance for accurate calibration at high-altitude locations. Our results are consistent with previous studies emphasizing the criticality of the accurate CCN calibration for the lower supersaturations.

KEYWORDS: Aerosol hygroscopicity; Aerosol–cloud interaction; Cloud droplets; Cloud microphysics; Instrumentation/sensors; Measurements

1. Introduction

Atmospheric aerosols particles, which act as cloud condensation nuclei (CCN), play a crucial role in modulating the global hydrological cycle and climate by influencing formation, abundance and lifetime of clouds, and precipitation (Seinfeld and Pandis 2012; Lohmann and Feichter 2005). The activation of aerosol particles as CCN is mainly dependent on the particle size, chemical composition, and water vapor supersaturation available in the atmosphere (Andreae et al. 2005; Andreae and Rosenfeld 2008; McFiggans et al. 2006). It is important to study the dependence of CCN concentration on aerosol size distribution under different water vapor supersaturation conditions for quantitative assessment of aerosol impact on cloud and precipitation formation, and to better understand the role of cloud in modulating the current and future climate change. Thus, the aerosol–cloud–precipitation interaction together represents the largest uncertainty in the current and future understanding of the climate change (Andreae and Rosenfeld 2008). Numerous studies focusing on understanding the determining factors for activation of aerosol particles into CCN under varied atmospheric conditions have been carried out in the past few years (Roberts et al. 2006; Petters and Kreidenweis 2007; Yum et al. 2007; Shilling et al. 2007; Gunthe et al. 2009, 2011; Rose et al. 2008; Pöhlker et al. 2016, 2018; Andreae et al. 2005; Andreae and Rosenfeld 2008). The continuous-flow streamwise thermal gradient Cloud Condensation Nuclei Counter (CCNC) by the Droplet Measurement Technologies (DMT), based on the design of Roberts and Nenes (2005) and Lance et al. (2006), is the most commonly used instrument for robust and reliable measurements of CCN properties of the atmospheric aerosols worldwide. For different operating conditions like changes in pressure, temperature, and flow inside the CCNC, the effective supersaturation actually generated in the CCN column will show different degree of deviations with respect to the supersaturation level nominally set in the instrument. It is therefore essential to perform careful calibration of the instrument, prior to performing ambient or laboratory experiments, for ensuring high accuracy of CCN measurement data.

Raj's current affiliation: Multiphase Chemistry and Biogeochemistry Departments, Max Planck Institute for Chemistry, Mainz, Germany.

Corresponding authors: Aishwarya Singh, aishwarya.singh129@gmail.com; Sachin S. Gunthe, s.gunthe@iitm.ac.in

DOI: 10.1175/JTECH-D-22-0092.1

TABLE 1. Summary of the location, altitude, campaign period, and calibration equation for 16 calibration experiments.

Location	Alt (m MSL)	Campaign period	Calibration equation	Source
Mainz	119	2005/06 (avg of 6 campaigns)	$y = 0.0754x - 0.1217$	Personal communication
Guangzhou	67	1 Jul 2006	$y = 0.0832x - 0.0903$	Rose et al. (2010)
Beijing	52	10 Aug 2006	$y = 0.079x - 0.1069$	Gunthe et al. (2011)
Jungfraujoch	3466	10 Feb 2007	$y = 0.0490x - 0.0760$	Rose et al. (2008)
Amazon	48	February 2008	$y = 0.0789x - 0.0909$	Gunthe et al. (2009)
Mainz	119	8 May 2010	$y = 0.0925x - 0.1464$	Personal communication
Mainz	119	10 May 2010	$y = 0.0817x - 0.1375$	Personal communication
Mainz	119	10 and 11 May 2010	$y = 0.0803x - 0.1272$	Personal communication
Mainz	119	12 May 2010 (a)	$y = 0.0671x - 0.1063$	Personal communication
Mainz	119	12 May 2010 (b)	$y = 0.0689x - 0.1154$	Personal communication
Mainz	119	17 May 2012	$y = 0.0766x - 0.1175$	Personal communication
Delhi	227	2 Feb 2018	$y = 0.056x - 0.031$	Raj et al. (2021)
Chennai	6.7	4 Jan 2019	$y = 0.0692x - 0.0699$	IIT Madras campaign
Chennai	6.7	Dec 2019	$y = 0.0701x - 0.0567$	IIT Madras campaign
Chennai	6.7	17 May 2020	$y = 0.072x - 0.061$	IIT Madras campaign
Munnar	1600	6 July 2021	$y = 0.039x - 0.027$	IIT Madras campaign

The aerosol particle size and hygroscopicity (the ability of an aerosol particle to uptake the water), which depend on the chemical composition of the aerosols, are the two most important factors which determine whether a particle is able to activate as CCN or not (Petters and Kreidenweis 2007). For highly accurate estimation of the effective supersaturation generated in the CCN column and other subsequent parameters further derived, including single hygroscopicity parameter κ, it is very important to have the accurate calibration of the DMT-CCNC using known salt particles of ammonium sulfate [$(NH_4)_2SO_4$] or sodium chloride (NaCl), as the CCN activation of these salts using Kohler theory is relatively well established and accurately explained in terms of critical dry diameter and corresponding critical supersaturation (Rose et al. 2008). For example, if the critical dry diameter is known for a given salt, using Kohler theory, the critical effective supersaturation is accurately estimated and vice versa. More details about the calibration method, various parameterizations used for the Kohler model, and other details can be found at Rose et al. (2008). The accurate and robust calibration of the CCNC poses various experimental and theoretical challenges, including experimental setup, and requires additional instruments such as scanning mobility particle sizer (SMPS) for size selecting the aerosols. The lack of robust calibration data to estimate the effective supersaturation during ambient measurements of CCN properties of aerosols often leads to erroneous estimates of the various CCN properties, including that of simple CCN number concentration. Owing to experimental difficulties and theoretical complexities associated with the CCNC calibration, often it is difficult to effectively interpret and poses questions on the reliability of the CCN data reported in the literature. Following upon this motivation, in this study we present the analysis of 16 different CCNC calibrations carried out under contrasting environments and varying conditions to derive one global average calibration line and corresponding equation. We further verify the usefulness and accuracy of estimated global line by performing the sensitivity analysis of reported effective supersaturation and estimated κ. The study also attempts to improve the global calibration equation by further classification of the data based on the altitude, as a proxy for changes in ambient pressure, and proposes the need of more calibrations at higher altitudes, particularly in the tropical Indian region, where dozens of CCNC are currently operated.

2. Methods

The experimental CCNC calibration data from 8 contrasting environmental conditions corresponding to 16 CCNC calibrations across the world at different periods have been analyzed in this study: namely, Mainz (average of 6 calibrations done in 2005/06), Guangzhou (1 July 2006), Beijing (10 August 2006), Jungfraujoch (10 February 2007), Amazon (February 2008), Mainz (8 May 2010), Mainz (10 May 2010), Mainz (11 May 2010), Mainz [12 May 2010 (a)], Mainz [12 May 2010 (b)], Mainz (17 May 2012), Delhi (2 February 2018), Chennai (4 January 2019), Chennai (December 2019), Chennai (17 May 2020), and Munnar (6 July 2021). A total of three instruments were used for the 16 calibration experiments listed. The experimental locations experience a diverse range of atmospheric conditions, which are expected to reflect in the calibration data. To consider the strong dependency of the effective supersaturation generated in the CCNC on the pressure difference owing to altitude, the experimental data under consideration were associated with a uniform CCN flow rate of 0.5 L min^{-1} except for Jungfraujoch, which is 0.8 L min^{-1}. The details of the calibrations experiments like location, altitude, campaign period, and calibration equations are given in Table 1. The detailed methodology, calibration setup, process, various corrections required for the obtained data, theoretical consideration, and various arameterizations are discussed in Rose et al. (2008). Briefly, the supersaturation in the CCNC column is generated by maintaining a temperature difference between the top and bottom of the CCNC controlled by the thermoelectric coolers (TECs), which are referred as T1 (a the top of CCNC column), T2 (in the middle of CCNC column), and T3 (at the bottom of CCNC column). The difference in the temperature between the top and bottom of the CCN column dT (T3 − T1), is set to a value

generally in the range of 2–17 K. Each unique value dT corresponds to a particular supersaturation set inside the column and experiments at a particular dT are referred to as a scan. For every scan or value of the dT, corresponding to set supersaturation, the diameter of aerosol particles entering the CCN column is varied by a differential mobility analyzer (DMA) nominally in the range of 20–350 nm. At a particular diameter set by the DMA, the total number concentration of particles, referred to as condensation nuclei (CN) is measured using a condensation particle counter (CPC). Further, the total number of CN which get activated as CCN in the CCN column is measured by an optical particle counter (OPC) at the exit of the CCNC column. The above procedure is repeated for different supersaturations set inside the CCN column. Thus, at the end of the experiments, CN concentration data at different diameters set by the DMA and the corresponding CCN concentrations at different supersaturation are obtained. The data are subjected to various correction procedures as discussed in Rose et al. (2008). The ratio of the number of particles activated as CCN to CN is defined as CCN efficiency. The plot of CCN efficiency versus diameter for each scan corresponding to a particular supersaturation gives an S-shaped curve known as the CCN efficiency spectra. This curve is fitted to a cumulative Gaussian distribution function to obtain various fitting parameters, one of which is the activation diameter—the critical dry particle diameter for CCN activation. For the determined activation diameter, the effective supersaturation S_{eff} practically present in the CCN column is calculated using Kohler theory; S_{eff} practically depends on the flow rate, ambient pressure, sample temperature, and the temperature gradient dT (Rose et al. 2008), which is further the function of the room temperature. It is important to note that the temperature at the top of the CCNC column is strongly dependent and adjusted based on the room temperature (Rose et al. 2008; Thalman et al. 2017); therefore, it is strongly recommended that the operating temperature of the CCNC should be kept as constant as possible. Thereafter, a linear calibration function, $S_{\text{eff}} = k_s dT + S_o$ is thus obtained from a least squares fit of S_{eff} and dT, where k_s and S_o are the slope and y intercept of the calibration line, respectively. This function is used as the calibration equation to determine the S_{eff} obtained inside the CCNC for the ambient CCN analysis, where the dT is (T3 − T1) from the CCNC. Figure 1 shows an exemplary calibration line from CCN calibration experiments conducted at the Natural Aerosol and Bioaerosol High Altitude laboratory (NABHA) at Munnar (10.0930°N, 77.0681°E; 1600 m MSL), India, on 6 July 2021.

As observed in Table 1, the data for this study have been obtained from published literature as well as various campaigns. S_{eff} and dT data were directly obtained from the cited literature for Beijing, Guangzhou, Jungfraujoch, and Amazon. For the other locations, the calculation procedure and corrections described above were adopted for the raw CCN calibration experimental data to obtain the respective calibration equations. Thus, the linear calibration function was fitted to the compiled data points for S_{eff} and dT for all the calibration experiments to obtain the global calibration equation. The applicability of this global calibration equation was inspected by its application to ambient CCN experimental data, available for Beijing, Chennai, Delhi, Munnar, Jungfraujoch, Amazon,

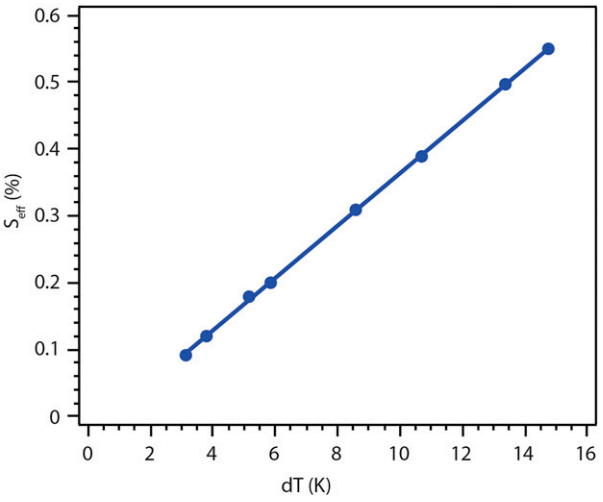

FIG. 1. Exemplary calibration line obtained from S_{eff} and dT values from a laboratory calibration experiment performed at Munnar using ammonium sulfate on 6 Jul 2021 ($N = 8$; $R^2 = 0.99$).

and Guangzhou. The experimental data, however, required corrections as mentioned earlier in the procedure for calibration. The data were first corrected for doubly charged particles with the same electrical mobility, but larger diameter. These doubly charged particles may infiltrate the DMA sample airflow as singly charged particles, for a set electrical mobility. Doubly charged particles could potentially alter the critical dry particle diameter by distorting the CCN efficiency spectra and were hence corrected using the size distribution. Transfer function correction was further applied to account for the limitation of particle size resolution achievable with the transfer function of the DMA. After performing the above corrections, a cumulative Gaussian distribution was fit to the ambient CCN efficiency curve to obtain the activation diameter as discussed earlier. Each spectra, which is measured provided a pair of S_{eff} and critical dry diameter, was then used to calculate κ, the single hygroscopicity parameter from the kappa-Kohler theory (Petters and Kreidenweis 2007). All the calculations were then performed by using the single (global) calibration line to obtain the S_{eff} based on the dT values given in the literature. Further analysis is performed by classifying the data based on altitude and calculating the calibration line separately for high-altitude and low-altitude regions, considering a threshold altitude of 1000 m. Out of all the locations, Jungfraujoch in Switzerland (3450 m MSL) and Munnar in India (1500 m MSL) were thus classified as high-altitude regions while the rest fall under low-altitude regions. The comparison of S_{eff} and κ is repeated for these cases as well.

3. Results and discussion

Figure 2 shows the scatterplot of S_{eff} versus dT for all the calibration experiments, with data points marked in a particular color corresponding to the calibration performed at a given location. A linear equation was fitted to the scatter, to obtain the global calibration equation as $S_{\text{eff}} = 0.07dT - 0.10$.

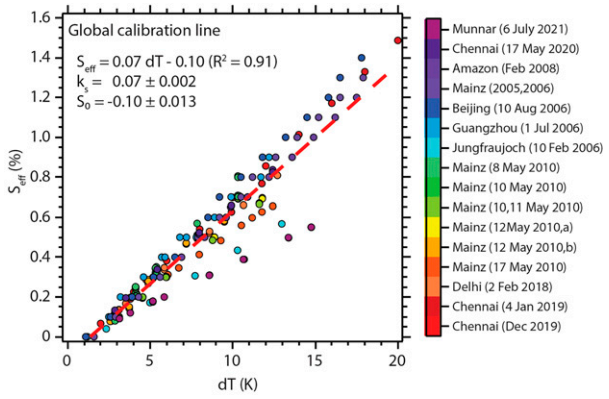

FIG. 2. Global average calibration line: the dashed red line represents the global average calibration line obtained from the best fit of the 223 data points from 16 calibration experiments conducted at contrasting environments across the globe. The data points are color coded on the basis of location and time of the calibration experiment as shown in the legend.

Considering the nature of the experimental studies, which were performed in regions of diverse conditions of temperature and pressure, a correlation of fit of 0.91 (R^2 = 0.91; N = 223) was obtained. The fitted slope and intercept, k_s and S_o, were observed to have a standard deviation of 0.002 and 0.013, respectively. The data points corresponding to different field campaigns are observed to exhibit very less scatter from the fitted line, which is also indicated by the observed high correlation of fit. However, the data points corresponding to the high-altitude locations—Jungfraujoch (3466 m MSL) and Munnar (1600 m MSL)—were observed to stand apart from the general trend of the global calibration line. This observation is consistent with previous studies that have reported a lower slope of the calibration line for high-altitude locations compared to that observed at low altitudes, due to the effect of ambient pressure (Rose et al. 2008).

To investigate the significance of altitude or, equivalently, the ambient pressure on the calibration line, a new average linear calibration equation was fitted separately for the high- and low-altitude points. Locations at an altitude greater than 1000 m MSL (Munnar and Jungfraujoch, in this study) were classified as high-altitude locations. The scatterplot of S_{eff} versus dT for both categories are displayed in Fig. 3. Figure 3a shows the scatterplot for low-altitude locations, for which the average linear calibration equation was determined to be $0.08dT - 0.11$ with a correlation of fit of 0.98. The fitted slope and intercept, k_s and S_o were observed to have a standard deviation of 0.001 and 0.007, respectively. Similarly, Fig. 3b shows the scatterplot for high-altitude locations, for which the average linear calibration equation was determined to be $0.04dT - 0.04$ with a correlation of fit of 0.98. The fitted slope and intercept, k_s and S_o, were observed to have a standard deviation of 0.002 and 0.015, respectively. Thus, the correlation of fit improved significantly from 0.91 to 0.98 when high-altitude locations were separated from the rest of the data. This suggests that ambient pressure significantly influences the linear calibration equation, and hence, CCN measurements at high-altitude locations need to be supplemented with high-altitude calibration experiments to ensure the accuracy of the measurements. Since varied ranges of temperatures are not observed to drastically modify the scatter of points in the low-altitude locations in Fig. 3a, the average calibration equation may be used effectively where calibration experiments are not feasible.

The results of the ambient data calculations for Beijing, Chennai, Delhi, Munnar, Jungfraujoch, Amazon, and Guangzhou using different calibration equations are summarized in Table 2. The effective supersaturation S_{eff}, supersaturation obtained using global and altitude-based average calibration lines (S_g and S_{avg}, respectively), their relative percentage differences, single hygroscopicity parameter kappa (κ), kappa obtained using global calibration line (κ_g) and average calibration line (κ_{avg}), and their relative percentage differences are tabulated. The results clearly show that the κ_{avg} predicted using the average calibration line is showing good agreement with that calculated using the local calibration equation with low relative uncertainties. Also, the prediction of κ improves when calculated using the average calibration equation κ_{avg} over the global calibration equation κ_g. Thus, the improvement

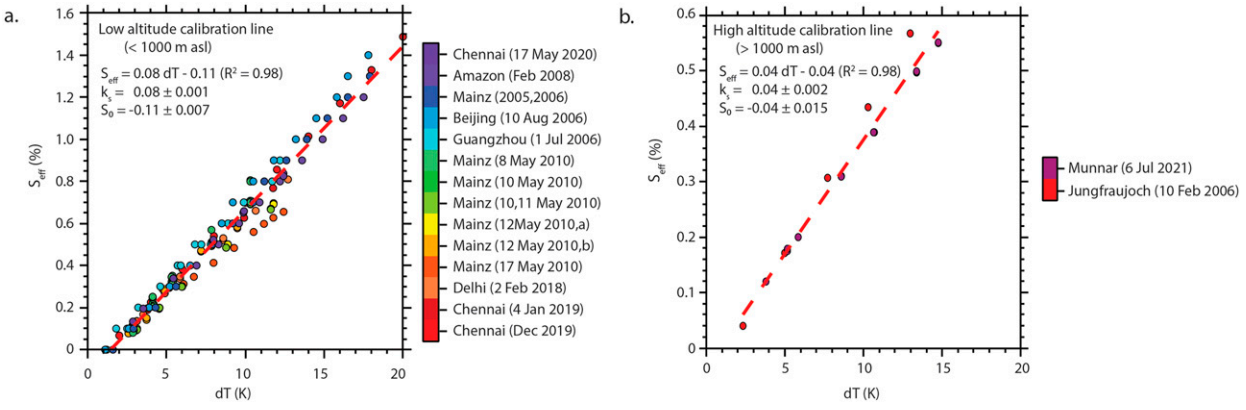

FIG. 3. Separate calibration lines as based on altitude. Average calibration lines were plotted separately (a) for elevation < 1000 m MSL with data from 14 calibration experiments and (b) for elevation > 1000 m MSL with data from 2 calibration experiments.

TABLE 2. Results of ambient CCN analysis carried out for seven different locations: Beijing (2006), Chennai (2019), Delhi (2018), Munnar (2021), Jungfraujoch (2007), Amazon (2008), and Guangzhou (2006). The tabulated quantities include the effective supersaturation obtained in the CCN column S_{eff} which is obtained by using local calibration equation for each experiment, supersaturation obtained using global average calibration equation and altitude-based average calibration equation S_g and S_{avg}, respectively, and their relative percentage difference with respect to S_{eff} ($\Delta S_g/S_{eff}$% and $\Delta S_{avg}/S_{eff}$%, respectively). The single hygroscopicity parameter κ value obtained using respective local calibration equations, kappa value which is obtained using global and altitude-based average calibration equations κ_g and κ_{avg}, respectively, and their relative percentage differences with respect to original kappa value ($\Delta\kappa_g/\kappa$% and $\Delta\kappa_{avg}/\kappa$%, respectively) are also given in the table.

dT	S_{eff}	D_{50}	S_g	$\Delta S_g/S_{eff}$%	S_{avg}	$\Delta S_{avg}/S_{eff}$%	κ	κ_g	$\Delta\kappa_g/\kappa$%	κ_{avg}	$\Delta\kappa_{avg}/\kappa$%
					Beijing						
1.97	0.05	163.27	0.04	10.33	0.04	17.06	1.36	1.69	24.35	1.97	45.38
4.48	0.25	80.21	0.23	7.83	0.24	4.67	0.45	0.53	17.74	0.50	10.06
6.97	0.44	61.04	0.41	7.55	0.43	3.32	0.34	0.40	17.16	0.37	7.05
9.47	0.64	48.74	0.59	7.45	0.62	2.81	0.31	0.36	16.96	0.32	5.94
11.95	0.84	41.09	0.78	7.40	0.82	2.54	0.29	0.34	16.87	0.31	5.36
					Chennai						
3.45	0.17	118.09	0.15	9.97	0.15	9.49	0.37	0.45	23.56	0.44	22.36
4.17	0.22	113.62	0.21	6.25	0.21	4.64	0.24	0.27	13.88	0.26	10.04
6.15	0.36	100.08	0.35	1.58	0.36	1.47	0.12	0.12	3.30	0.12	2.95
6.71	0.39	91.10	0.39	0.84	0.40	2.44	0.12	0.13	1.73	0.12	4.81
7.97	0.48	82.93	0.48	0.39	0.50	4.04	0.12	0.12	0.79	0.11	7.88
9.25	0.57	75.55	0.58	1.25	0.60	5.16	0.10	0.10	2.56	0.09	9.98
10.35	0.65	75.77	0.66	1.79	0.68	5.87	0.08	0.08	3.72	0.07	11.50
11.14	0.70	74.94	0.72	2.12	0.75	6.31	0.08	0.07	4.46	0.07	12.44
12.42	0.79	71.32	0.81	2.55	0.84	6.86	0.07	0.07	5.43	0.06	13.69
					Delhi						
2.89	0.13	151.67	0.11	14.95	0.11	14.33	0.25	0.34	38.38	0.34	36.40
4.17	0.20	111.42	0.21	1.27	0.21	4.44	0.25	0.25	2.50	0.23	8.36
6.07	0.31	84.52	0.34	11.46	0.36	16.24	0.25	0.20	19.68	0.18	26.22
6.70	0.34	81.14	0.39	13.46	0.41	18.55	0.25	0.19	22.58	0.17	29.18
7.97	0.42	72.50	0.48	16.43	0.51	21.99	0.23	0.17	26.61	0.15	33.28
9.25	0.49	69.27	0.58	18.57	0.61	24.46	0.19	0.14	29.47	0.12	36.20
10.51	0.56	65.64	0.67	20.13	0.70	26.27	0.18	0.12	31.56	0.11	38.36
11.76	0.63	62.21	0.76	21.34	0.80	27.67	0.16	0.11	33.17	0.10	40.00
					Munnar						
2.92	0.09	142.99	0.11	30.42	0.08	3.65	0.66	0.39	41.24	0.71	7.72
3.55	0.11	129.35	0.16	43.20	0.11	1.70	0.58	0.28	51.32	0.60	3.49
4.82	0.16	97.82	0.25	56.92	0.16	0.39	0.64	0.26	59.52	0.64	0.78
5.45	0.19	88.24	0.30	61.07	0.19	1.03	0.62	0.24	61.60	0.60	2.02
7.98	0.28	80.04	0.48	70.40	0.29	2.45	0.40	0.14	66.12	0.38	4.75
9.89	0.36	67.95	0.62	74.05	0.37	3.01	0.38	0.12	67.66	0.36	5.79
12.42	0.46	52.51	0.81	77.06	0.47	3.46	0.48	0.15	68.69	0.45	6.62
					Jungfraujoch						
2.40	0.08	171.70	0.08	4.74	0.06	20.64	0.43	0.48	10.21	0.69	58.82
3.49	0.17	114.50	0.15	8.83	0.11	36.76	0.32	0.38	20.37	0.79	150.39
4.66	0.27	88.40	0.24	10.69	0.16	42.26	0.27	0.34	25.50	0.82	200.69
6.90	0.46	65.10	0.40	12.00	0.25	46.11	0.23	0.30	29.43	0.81	246.28
9.30	0.66	52.80	0.58	11.96	0.35	47.43	0.21	0.27	29.49	0.77	265.18
					Amazon						
2.42	0.1	199	0.08	23.32	0.07	26.30	0.17	0.26	49.49	0.31	76.12
3.56	0.19	127.9	0.16	15.63	0.16	14.98	0.18	0.24	31.68	0.24	34.33
4.7	0.28	105.3	0.24	12.88	0.25	10.94	0.15	0.19	26.23	0.18	23.08
6.98	0.46	82.8	0.41	10.61	0.43	7.60	0.11	0.14	22.09	0.13	14.82
11.54	0.82	54.6	0.75	9.06	0.78	5.32	0.12	0.15	19.47	0.13	9.65
					Guangzhou						
1.98	0.07	189.5	0.05	33.63	0.04	37.56	0.44	0.99	127.07	1.12	156.57
4.51	0.27	81.4	0.23	14.60	0.24	12.12	0.35	0.48	37.25	0.45	29.59
7.01	0.47	59.4	0.41	11.95	0.43	8.56	0.3	0.38	29.21	0.35	19.76
9.51	0.67	48.9	0.6	10.88	0.62	7.12	0.26	0.33	26.27	0.3	16.14
12.01	0.87	40.9	0.78	10.31	0.81	6.35	0.26	0.33	24.74	0.3	14.28
17.01	1.27	31.5	1.15	9.70	1.2	5.53	0.27	0.33	23.13	0.3	12.36

in the prediction of kappa after the classification of calibration data based on altitude substantiates the earlier observation of the dominant effect of pressure on the calibration equation. The maximum relative percentage difference in average S_{eff} and κ from original values using average calibration equation for $S_{\text{eff}} > 0.1$, respectively, are 4.67% and 10.06% (Beijing), 9.49% and 22.36% (Chennai), 27.67% and 40% (Delhi), 1.7% and 3.49% (Munnar), 47.43% and 265.18% (Jungfraujoch), 14.98% and 34.33% (Amazon), and 12.12% and 29.59% (Guangzhou). Unlike the other locations, the huge difference in s_{avg} and κ_{avg} from original values for Jungfraujoch is due to the change in the flow used in CCN column, which has already been discussed in Rose et al. (2008) and Thalman et al. (2017). Except for Jungfraujoch, where the ambient CCN measurements were taken at a flow rate of 0.8 L min^{-1}, all other experiments were carried out at a flow rate of 0.5 L min^{-1}.

A significant difference in the kappa predictions using global and local calibration equations is observed for lower supersaturation, $S_{\text{eff}} < 0.1$. Previous studies have reported uncertainties in the linearity of the relationship between S_{eff} and dT for supersaturation less than 0.1 (Rose et al. 2008). Hence, our observations for $S_{\text{eff}} < 0.1$ are not expected to produce major uncertainty in the proposed average calibration equation. Thus, it is important to note that special care has to be exercised while analyzing and interpreting the calibration data for lower supersaturations.

4. Conclusions

Data from 16 calibration experiments from various locations across the globe were used to obtain a global calibration equation—$S_{\text{eff}} = 0.07dT - 0.10$—by a linear fit to S_{eff} versus dT data for all the calibration experiments. Considering that the experiments had been performed at regions covering a wide range of temperature, altitude, and pressure conditions, an impressive correlation of fit of 0.91 was observed. Our calculations suggest good compatibility of a global average calibration equation with respect to the local equations, especially at low altitudes. Hence, such an average calibration equation may be effectively used for analyzing the size-resolved CCN data where robust and accurate calibration is not possible, instead of individual equations for a particular location. This may be especially useful during CCN studies where performing calibration experiments may not be feasible owing to the logistical issues.

The locations were further separated based on altitude (considering a threshold of altitude > 1000 m MSL as high-altitude locations), and average linear calibration equations were fitted separately for the high- and low-altitude points. Prediction of parameters like S_{eff} and κ using the global and altitude-based calibration equations were analyzed and compared with those predicted using the respective local calibration equations for the different campaigns. Improvement in the predictions was observed after the altitude-based classification, and thus, pressure was identified to have a major influence on the calibration equation as reported by the previous studies.

Considering the fact that the calibrations have been performed in wide temperature conditions, the ambient temperature would also have an effect on the effective supersaturation attained in CCNC, which is very evident from the previous studies (Rose et al. 2008; Thalman et al. 2017). Even though in a short span of three months, multiple calibration experiments have been performed in our recent campaign in Munnar (2021), we maintained a constant room temperature (296 K) so that this effect could be minimized. Several other factors could affect the effective supersaturation attained in CCNC, such as the number of particles (a very high number of particles leads to a higher number of doubly charged particles), DMA transfer function, and long-term changes in instrument properties (Rose et al. 2008).

Previously, in literature, many CCN studies have been carried out without considering the calibration of the instrument. Because of the tedious process of calibration, except for research groups that are experts in using the instrument, most would directly do ambient measurements without calibrating the CCN counter. This paper is limited to understanding the applicability of using an average calibration equation in place of an individual calibration equation, where calibration is hindered by the required facilities and expertise, with a minimum deviation in effective supersaturation attained in the CCN column. However, for CCN measurements that require very high accuracy, especially at high altitudes, experimental calibration is preferable. Nevertheless, collective efforts to compile CCN calibration data from many more experimental studies may be beneficial in fine-tuning the global calibration equation for future use. The accurate ambient measurement of the CCN data is essential for climate models, which will eventually help to reduce the aerosol–cloud–precipitation related uncertainty to predict better the climate change forcing expected by the end of this century. Our analysis presented here may be useful in inferring the accurate CCN concentration under size-resolved CCN measurements and subsequent parameterizations, including the aerosol hygroscopicity, and will help in improved parameterization for use in prognostic models.

Acknowledgments. Author Gunthe gratefully acknowledges funding from the Ministry of Earth Sciences (MoES; Sanction MoES/16/20/12-RDEAS dated 31 March 2014), government of India, for the purchase of the Cloud Condensation Nuclei Counter (CCNC). This work was supported by partial funding from the MoES [Sanction MoES/16/04/2017-APHH (PROMOTE)], government of India, and the Department of Science and Technology (Sanction DST/CCP/CoE/141/2018C), government of India. This work was also partially supported by the U.K. Natural Environment Research Council with Grant Reference Numbers NE/P016480/1 and NE/P016472/1. Gunthe gratefully acknowledges the support from the Max Planck Institute for Chemistry, Mainz, Germany, for considering the request to use the CCN calibration data for the experiments, which were performed there. Author Singh gratefully acknowledges the Prime Minister's Research fellowship (PMRF) for doctoral research from Ministry of Education, government of India.

Data availability statement. All of the data used in this study can be made available upon request to the corresponding author.

REFERENCES

Andreae, M. O., and D. Rosenfeld, 2008: Aerosol–cloud–precipitation interactions. Part 1. The nature and sources of cloud-active aerosols. *Earth-Sci. Rev.*, **89**, 13–41, https://doi.org/10.1016/j.earscirev.2008.03.001.

——, C. D. Jones, and P. M. Cox, 2005: Strong present-day aerosol cooling implies a hot future. *Nature*, **435**, 1187–1190, https://doi.org/10.1038/nature03671.

Gunthe, S. S., and Coauthors, 2009: Cloud condensation nuclei in pristine tropical rainforest air of Amazonia: Size-resolved measurements and modeling of atmospheric aerosol composition and CCN activity. *Atmos. Chem. Phys.*, **9**, 7551–7575, https://doi.org/10.5194/acp-9-7551-2009.

——, and Coauthors, 2011: Cloud condensation nuclei (CCN) from fresh and aged air pollution in the megacity region of Beijing. *Atmos. Chem. Phys.*, **11**, 11 023–11 039, https://doi.org/10.5194/acp-11-11023-2011.

Lance, S., A. Nenes, J. Medina, and J. N. Smith, 2006: Mapping the operation of the DMT continuous flow CCN counter. *Aerosol Sci. Technol.*, **40**, 242–254, https://doi.org/10.1080/02786820500543290.

Lohmann, U., and J. Feichter, 2005: Global indirect aerosol effects: A review. *Atmos. Chem. Phys.*, **5**, 715–737, https://doi.org/10.5194/acp-5-715-2005.

McFiggans, G., and Coauthors, 2006: The effect of physical and chemical aerosol properties on warm cloud droplet activation. *Atmos. Chem. Phys.*, **6**, 2593–2649, https://doi.org/10.5194/acp-6-2593-2006.

Petters, M. D., and S. M. Kreidenweis, 2007: A single parameter representation of hygroscopic growth and cloud condensation nuclei activity. *Atmos. Chem. Phys.*, **7**, 1961–1971, https://doi.org/10.5194/acp-7-1961-2007.

Pöhlker, M. L., and Coauthors, 2016: Long-term observations of cloud condensation nuclei in the Amazon rain forest—Part 1: Aerosol size distribution, hygroscopicity, and new model parametrizations for CCN prediction. *Atmos. Chem. Phys.*, **16**, 15 709–15 740, https://doi.org/10.5194/acp-16-15709-2016.

——, and Coauthors, 2018: Long-term observations of cloud condensation nuclei in the Amazon rain forest—Part 2: Variability and characteristic differences under near-pristine, biomass burning, and long-range transport conditions. *Atmos. Chem. Phys.*, **18**, 10 289–10 331, https://doi.org/10.5194/acp-18-10289-2018.

Raj, S. S., and Coauthors, 2021: Planetary boundary layer height modulates aerosol—Water vapor interactions during winter in the megacity of Delhi. *J. Geophys. Res. Atmos.*, **126**, e2021JD035681, https://doi.org/10.1029/2021JD035681.

Roberts, G. C., and A. Nenes, 2005: A continuous-flow streamwise thermal-gradient CCN chamber for atmospheric measurements. *Aerosol Sci. Technol.*, **39**, 206–221, https://doi.org/10.1080/027868290913988.

——, G. Mauger, O. Hadley, and V. Ramanathan, 2006: North American and Asian aerosols over the eastern Pacific Ocean and their role in regulating cloud condensation nuclei. *J. Geophys. Res.*, **111**, D13205, https://doi.org/10.1029/2005JD006661.

Rose, D., S. S. Gunthe, E. Mikhailov, G. P. Frank, D. Ulrike, M. O. Andreae, and U. Pöschl, 2008: Calibration and measurement uncertainties of a continuous-flow cloud condensation nuclei counter (DMT-CCNC): CCN activation of ammonium sulfate and sodium chloride aerosol particles in theory and experiment. *Atmos. Chem. Phys.*, **8**, 1153–1179, https://doi.org/10.5194/acp-8-1153-2008.

——, and Coauthors, 2010: Cloud condensation nuclei in polluted air and biomass burning smoke near the mega-city Guangzhou, China—Part 1: Size-resolved measurements and implications for the modeling of aerosol particle hygroscopicity and CCN activity. *Atmos. Chem. Phys.*, **10**, 3365–3383, https://doi.org/10.5194/acp-10-3365-2010.

Seinfeld, J. H., and S. N. Pandis, 2012: *Atmospheric Chemistry and Physics: From Air Pollution to Climate Change*. Wiley, 1232 pp.

Shilling, J. E., S. M. King, M. Mochida, D. R. Worsnop, and S. T. Martin, 2007: Mass spectral evidence that small changes in composition caused by oxidative aging processes alter aerosol CCN properties. *J. Phys. Chem. A*, **111**, 3358–3368, https://doi.org/10.1021/jp068822r.

Thalman, R., and Coauthors, 2017: CCN activity and organic hygroscopicity of aerosols downwind of an urban region in central Amazonia: Seasonal and diel variations and impact of anthropogenic emissions. *Atmos. Chem. Phys.*, **17**, 11 779–11 801, https://doi.org/10.5194/acp-17-11779-2017.

Yum, S. S., G. Roberts, J. H. Kim, K. Song, and D. Kim, 2007: Submicron aerosol size distributions and cloud condensation nuclei concentrations measured at Gosan, Korea, during the Atmospheric Brown Clouds–East Asian Regional Experiment 2005. *J. Geophys. Res.*, **112**, D22S32, https://doi.org/10.1029/2006JD008212.